IDENTIFICATION AND CONTROL OF ACOUSTIC RADIATION MODES

Arthur P. Berkhoff

University of Twente, Faculty of Electrical Engineering, P.O. Box 217, 7500 AE Enschede, The Netherlands
email: a.p.berkhoff@el.utwente.nl
and
TNO TPD, Acoustics Division, PO Box 155, 2600AD Delft, The Netherlands
email: berkhoff@tpd.tno.nl

Abstract

A formulation is given of reduced-order acoustic radiation sensors and reduced-order actuators for broadband sound fields. Methods are presented to determine these descriptions from measured data, and their application in systems for broadband active noise control is discussed. One application area is the reduction of sound radiated from plates with structural actuators and structural sensors, using measured or modeled versions of the most efficiently radiating patterns of a vibrating body, the so-called radiation modes. The second application of the radiation mode theory is in active noise barriers for the reduction of traffic noise. Without special precautions most of these systems suffer from spillover; a technique is given to arrive at good reductions at the error sensors with reduced spillover.

1 Introduction

In problems in which the radiated sound has to be reduced it is of interest to know the vibration patterns that radiate most efficiently (C.R.Fuller, S.J.Elliott and P.A.Nelson, 1996). In structural acoustics problems, one approach is to determine the radiation efficiency of each structural mode independently (W.T.Baumann, W.R.Saunders and H.H.Robertshaw, 1991). In many cases it may be more economic to rewrite the problem in terms of a set of virtual vibrations patterns that radiate sound most efficiently (G.V.Borgiotti, 1990; S.J.Elliott and M.E.Johnson, 1993). This approach can be used to arrive at sensing and actuation schemes with reduced order. A few practical implementations have been described in the literature (G.P.Gibbs, R.L.Clark, D.E.Cox and J.S.Vipperman, 2000; E.J.J.Doppenberg, A.P.Berkhoff and M.v.Overbeek, 2001). All these methods, also the practical implementations, are still based on models of acoustic radiation, such as the sound radiation from baffled plates. One reason is that it is not very easy to obtain the radiation modes in practice (A.P.Berkhoff, E.Sarajlic, B.S.Cazzolato and C.H.Hansen, 2001), at least not for monochromatic sound radiation. Recently, a modification of the radiation mode theory has been presented (A.P.Berkhoff,

2002), which allows robust identification of the radiation mode shapes by using a broadband formulation. In the present paper a formulation is given in the time domain in terms of operator notation and farfield descriptions. The conditions are given under which one of the measurement procedures leads to valid results.

2 Formulation of the problem

As discussed by many authors, such as (A.D.Pierce, 1989), the frequency domain sound field of a vibrating body in an acoustic fluid can be described by the Helmholtz integral equation. Upon solution of the equation for the pressure on the vibrating body, the Helmholtz equation can be used to evaluate the acoustic far field. In the time domain the integral equation for points $\mathbf{x}$ on the body $\mathcal{S}$ is given by

$$\frac{1}{2}p(\mathbf{x},t) = \int_{\mathbf{x}'\in\mathcal{S}} \left[\rho \frac{\partial_t v_k\left(\mathbf{x}', t - \frac{|\mathbf{x}-\mathbf{x}'|}{c}\right)}{4\pi|\mathbf{x}-\mathbf{x}'|} - \partial_k \frac{p\left(\mathbf{x}', t - \frac{|\mathbf{x}-\mathbf{x}'|}{c}\right)}{4\pi|\mathbf{x}-\mathbf{x}'|} \right] \nu'_k \mathrm{d}\mathbf{x}', \quad \mathbf{x}\in\mathcal{S} \tag{1}$$

with p and $v_k, k = 1,2,3$ the acoustic pressure and acoustic particle velocity, respectively, ρ the density of air, c the speed of sound, $\nu_k, k = 1,2,3$ the outward-pointing unit vector normal to the surface, and where t denotes time. The spatial coordinate is $\mathbf{x} = (x,y,z)$. Upon the solution of this equation, the pressure in the acoustic fluid in domain $\mathcal{D}$ can be computed with

$$p(\mathbf{x},t) = \int_{\mathbf{x}'\in\mathcal{S}} \left[\rho \frac{\partial_t v_k\left(\mathbf{x}', t - \frac{|\mathbf{x}-\mathbf{x}'|}{c}\right)}{4\pi|\mathbf{x}-\mathbf{x}'|} - \partial_k \frac{p\left(\mathbf{x}', t - \frac{|\mathbf{x}-\mathbf{x}'|}{c}\right)}{4\pi|\mathbf{x}-\mathbf{x}'|} \right] \nu'_k \mathrm{d}\mathbf{x}', \quad \mathbf{x}\in\mathcal{D} \tag{2}$$

In the far field we can make the approximation:

$$t - \frac{|\mathbf{x}-\mathbf{x}'|}{c} \rightarrow t - \frac{|\mathbf{x}|}{c} + \frac{\xi_q x'_q}{c} \quad |\mathbf{x}|\rightarrow\infty \tag{3}$$

where we have introduced the observation direction ξ_k

$$\xi_k = \frac{x_k}{|\mathbf{x}|} \tag{4}$$

In addition, the denominators can be approximated by $|\mathbf{x}|$ as $|\mathbf{x}|\rightarrow\infty$. The expression for the pressure becomes

$$\begin{aligned} p(\mathbf{x},t) = \frac{1}{4\pi|\mathbf{x}|}\int_{\mathbf{x}'\in\mathcal{S}} \Bigg[& \rho\partial_t v_k\left(\mathbf{x}', t - \frac{|\mathbf{x}|}{c} + \frac{\xi_q x'_q}{c}\right) + \\ & -\partial_k p\left(\mathbf{x}', t - \frac{|\mathbf{x}|}{c} + \frac{\xi_q x'_q}{c}\right)\Bigg] \nu'_k \mathrm{d}\mathbf{x}' \quad \mathbf{x}\in\mathcal{D}, |\mathbf{x}|\rightarrow\infty \end{aligned} \tag{5}$$

Let us define the farfield radiation patterns f and h by:

$$\{p, v_k\}(\mathbf{x},t) = \frac{\{f, h_k\}\left(\boldsymbol{\xi}, t - \frac{|\mathbf{x}|}{c}\right)}{4\pi|\mathbf{x}|} \tag{6}$$

Then,

$$f(\boldsymbol{\xi},t)=\int_{\mathbf{x}'\in\mathcal{S}}\left[\rho\partial_t v_k\left(\mathbf{x}',t+\frac{\xi_q x'_q}{c}\right)-\partial_k p\left(\mathbf{x}',t+\frac{\xi_q x'_q}{c}\right)\right]\nu'_k\mathrm{d}\mathbf{x}' \qquad \mathbf{x}\in\mathcal{D},|\mathbf{x}|\to\infty \tag{7}$$

Using

$$\partial_k p=-\frac{\xi_k}{c}\partial_t p,\quad |\mathbf{x}|\to\infty, \tag{8}$$

we can write

$$f(\boldsymbol{\xi},t)=\int_{\mathbf{x}'\in\mathcal{S}}\left[\rho\partial_t v_k\left(\mathbf{x}',t+\frac{\xi_q x'_q}{c}\right)-\frac{\xi_k}{c}\partial_t p\left(\mathbf{x}',t+\frac{\xi_q x'_q}{c}\right)\right]\nu'_k\mathrm{d}\mathbf{x}' \qquad \mathbf{x}\in\mathcal{D},|\mathbf{x}|\to\infty \tag{9}$$

The above expressions show that $f(\boldsymbol{\xi},t)$ is a function of the nomal velocity $v(\mathbf{x},t)$, where $v=v_k\nu_k$. We define the operator E by:

$$f=\mathsf{E}v=\mathsf{E}\{v(\mathbf{x},t)\}(\boldsymbol{\xi},t)=\int_{\tau\in\mathcal{T}}\mathrm{d}\tau\int_{\mathbf{x}\in\mathcal{S}}K(\boldsymbol{\xi},\mathbf{x},\tau)v(\mathbf{x},t-\tau)\mathrm{d}\mathbf{x} \tag{10}$$

An inner product on $\mathcal{S}$ is defined as

$$<v_1,v_2>=\int_{\mathbf{x}\in\mathcal{S}}v_1^*(\mathbf{x},t)v_2(\mathbf{x},t)\mathrm{d}\mathbf{x} \tag{11}$$

and an inner product over the angular sector Ω is defined as

$$[f_1,f_2]=\int_{\boldsymbol{\xi}\in\Omega}f_1^*(\boldsymbol{\xi},t)f_2(\boldsymbol{\xi},t)\mathrm{d}\boldsymbol{\xi} \tag{12}$$

The radiated power is defined as

$$W(\Omega)=\mathcal{E}[f,f] \tag{13}$$

where $\mathcal{E}$ is the expected value operator. We also define the adjoint operator E^+ by

$$[f,\mathsf{E}v]=<\mathsf{E}^+f,v> \tag{14}$$

Substitution of Eq. (10) in Eq. (14) shows that the adjoint operator E^+ is given by

$$v=\mathsf{E}^+f=\mathsf{E}^+\{f(\boldsymbol{\xi},t)\}(\mathbf{x},t)=\int_{\tau\in\mathcal{T}}\mathrm{d}\tau\int_{\boldsymbol{\xi}\in\Omega}K^*(\boldsymbol{\xi},\mathbf{x},\tau)f(\boldsymbol{\xi},t+\tau)\mathrm{d}\boldsymbol{\xi} \tag{15}$$

As compared to E, E^+ defines a complex conjugated, anti-causal system. The inner product evaluated from the radiation pattern f can be written as

$$[f,f]=<\mathsf{E}^+\mathsf{E}v,v> \tag{16}$$

The radiated power becomes

$$W(\Omega)=\mathcal{E}<\mathsf{E}^+\mathsf{E}v,v>= \int_{\mathbf{x}\in\mathcal{S}}\int_{\mathbf{x}'\in\mathcal{S}}\int_{\tau\in\mathcal{T}}\int_{\tau'\in\mathcal{T}}\int_{\boldsymbol{\xi}\in\Omega}K(\boldsymbol{\xi},\mathbf{x},\tau)K^*(\boldsymbol{\xi},\mathbf{x}',\tau')\mathcal{E}\left\{v(\mathbf{x}',t+\tau-\tau')v(\mathbf{x},t)\right\} \mathrm{d}\boldsymbol{\xi}\mathrm{d}\tau'\mathrm{d}\tau\mathrm{d}\mathbf{x}'\mathrm{d}\mathbf{x} \tag{17}$$

If we assume that any frequency dependence in the normal velocity $v(\mathbf{x},t)$ is incorporated in K and that, therefore, $v(\mathbf{x},t)$ can be considered to be temporally white, we can write

$$\mathcal{E}\left\{v(\mathbf{x}',t+\tau-\tau')v(\mathbf{x},t)\right\} = R_{vv}(\mathbf{x},\mathbf{x}')\delta(\tau-\tau') \tag{18}$$

and the radiated power becomes

$$W(\Omega) = \int_{\mathbf{x}\in\mathcal{S}}\int_{\mathbf{x}'\in\mathcal{S}}\int_{\tau\in\mathcal{T}}\int_{\boldsymbol{\xi}\in\Omega} K(\boldsymbol{\xi},\mathbf{x},\tau)K^*(\boldsymbol{\xi},\mathbf{x}',\tau)R_{vv}(\mathbf{x},\mathbf{x}') \mathrm{d}\boldsymbol{\xi}\mathrm{d}\tau\mathrm{d}\mathbf{x}'\mathrm{d}\mathbf{x} \tag{19}$$

which involves a Hermitian and positive definite operator $\mathsf{K}^+\mathsf{K}$ defined by

$$w = \mathsf{K}^+\mathsf{K}\{u\}(\mathbf{x}) = \int_{\mathbf{x}'\in\mathcal{S}}\int_{\tau\in\mathcal{T}}\int_{\boldsymbol{\xi}\in\Omega} K(\boldsymbol{\xi},\mathbf{x},\tau)K^*(\boldsymbol{\xi},\mathbf{x}',\tau)u(\mathbf{x}')\mathrm{d}\boldsymbol{\xi}\mathrm{d}\tau\mathrm{d}\mathbf{x}' \tag{20}$$

that defines a set of eigenvectors V_j on $\mathcal{S}$:

$$\int_{\mathbf{x}'\in\mathcal{S}}\int_{\tau\in\mathcal{T}}\int_{\boldsymbol{\xi}\in\Omega} K(\boldsymbol{\xi},\mathbf{x},\tau)K^*(\boldsymbol{\xi},\mathbf{x}',\tau)V_j(\mathbf{x}')\mathrm{d}\boldsymbol{\xi}\mathrm{d}\tau\mathrm{d}\mathbf{x}' = \lambda_j V_j(\mathbf{x}),\ j=1,2,\ldots,\mathbf{x}\in\mathcal{S} \tag{21}$$

or, expressed in operator notation:

$$\mathsf{K}^+\mathsf{K}V_j = \lambda_j V_j,\ \ j=1,2,\ldots \tag{22}$$

which identifies an orthonormal system of vibration patterns on $\mathcal{S}$:

$$< V_i, V_j >= \delta_{ij},\ \ j=1,2,\ldots \tag{23}$$

where δ_{ij} is the Kronecker delta. The eigenvalues of Eq. (22) are real and positive. The resulting control system is based on the minimization of the signals

$$\nu_j =< v, V_j >,\ \ j=1,2,\ldots \tag{24}$$

which can be weighted by a matrix of frequency dependent filters based on the radiation efficiency of the different V_j (A.P.Berkhoff, 2000).

3 Radiation modes obtained from measured data

The radiation modes as defined in this paper can be obtained once the kernel K is known. With direct measurement of this kernel in the frequency domain, using sources on or near the radiating surface (G.H.Koopmann and J.B.Fahnline, 1997), reliable results are often difficult to achieve(A.P.Berkhoff et al., 2001). Alternatively, the kernel can be obtained from broadband input-output data using system identification techniques (A.P.Berkhoff, 2002), such as subspace based techniques (P.v.Overschee and B.D.Moor, 1996), by applying a sufficient number of persistently exciting vibration patterns to the structure. System identification methods are also used in one of the examples. Sometimes it can be more efficient to exploit the underlying properties of the medium. In the following a relationship is given between nearfield quantities and

farfield quantities by defining two different states of the medium, state A and state B. This relationship can then be used to obtain the shapes V_j in a relatively straightforward manner. The two states A and B are described by the following equations (M.D.Verweij, 1995)

$$\partial_k p^A + \partial_t C_t\{\rho^A, v_k^A\} = {f'}_k^A \tag{25}$$
$$\partial_k v_k^A + \partial_t C_t\{\kappa^A, p^A\} = {q'}^A \tag{26}$$

$$\partial_k p^B + \partial_t C_t\{\rho^B, v_k^B\} = {f'}_k^B \tag{27}$$
$$\partial_k v_k^B + \partial_t C_t\{\kappa^B, p^B\} = {q'}^B \tag{28}$$

in which C_t denotes temporal convolution. For reasons of simplicity, the medium is assumed to be lossless. In a homogeneous medium, in which $\rho^A = \rho^B$ and $\kappa^A = \kappa^B$, we have the field reciprocity relation

$$\int_{\mathbf{x}\in\mathcal{S}} \left[C_t\{p^A, v_k^B\} - C_t\{v_k^A, p^B\}\right] \nu_k \mathrm{d}\mathbf{x} =$$
$$\int_{\mathbf{x}\in\mathcal{D}} \left[C_t\{{f'}_k^A, v_k^B\} + C_t\{p^A, {q'}^B\} - C_t\{v_k^A, {f'}_k^B\} - C_t\{{q'}^A, p^B\}\right] \mathrm{d}\mathbf{x} \tag{29}$$

If we take state A to be source free and state B as the state with a volume injection source ${q'}^B = q^B\delta(\mathbf{x} - \mathbf{x}^B)$, then we obtain

$$\int_{\mathbf{x}\in\mathcal{S}} \left[C_t\{p^A, v_k^B\} - C_t\{v_k^A, p^B\}\right] \nu_k \mathrm{d}\mathbf{x} = C_t\{p^A(\mathbf{x}^B)q^B\}, \;\; \mathbf{x}^B \in \mathcal{D} \tag{30}$$

If $\mathcal{S}$ denotes a rigid source then $v_k^B\nu_k$ vanishes on $\mathcal{S}$ and we have

$$\int_{\mathbf{x}\in\mathcal{S}} -C_t\{v_k^A, p^B\}\nu_k \mathrm{d}\mathbf{x} = C_t\{p^A(\mathbf{x}^B)q^B\}, \;\; \mathbf{x}^B \in \mathcal{D} \tag{31}$$

If $q^B(t)$ equals a temporal Dirac impulse at time $t = 0$ then the corresponding response $p^B(\mathbf{x}, t)$ equals the Green's function $g^B(\mathbf{x}, t)$ by definition. State A is taken to be the actual medium state, i.e. $v_k^A = v_k$ and $p^A = p$. Then the following equation holds:

$$\int_{\mathbf{x}\in\mathcal{S}} -C_t\{v_k, g^B\}\nu_k \mathrm{d}\mathbf{x} = p(\mathbf{x}^B), \;\; \mathbf{x}^B \in \mathcal{D} \tag{32}$$

This shows that the pressure p is related to the normal velocity $v_k\nu_k$ and the Green's function $g^B = g(\mathbf{x}, \mathbf{x}^B, t)$ on the radiator $\mathcal{S}$, which is obtained by measuring the pressure on $\mathcal{S}$ in response to an impulsive volume injection source in the farfield. Alternatively, if suitable excitation signals are used then the desired transfer functions can be obtained by system identification. If $\mathbf{x}^B$ is in the farfield with respect to $\mathcal{S}$ then the Green's function can be written as $g(\mathbf{x}, \mathbf{x}^B, t + \frac{|\mathbf{x}^B|}{c}) = g(\mathbf{x}, \boldsymbol{\xi}, t + \frac{|\mathbf{x}^B|}{c})$. Use of Eq. (6) leads to

$$f^B(\boldsymbol{\xi}, t) = 4\pi|\mathbf{x}^B| \int_{\tau\in\mathcal{T}} \mathrm{d}\tau \int_{\mathbf{x}\in\mathcal{S}} g\left(\mathbf{x}, \boldsymbol{\xi}, t + \frac{|\mathbf{x}^B|}{c}\right) v(\mathbf{x}, t - \tau)\mathrm{d}\mathbf{x} \tag{33}$$

which shows that we have the relation

$$K(\boldsymbol{\xi}, \mathbf{x}) = -4\pi|\mathbf{x}_B|g^B\left(\mathbf{x}, \boldsymbol{\xi}, t + \frac{|\mathbf{x}^B|}{c}\right) \tag{34}$$

Hence, provided $\mathcal{S}$ is rigid, $K(\boldsymbol{\xi}, \mathbf{x})$ can be obtained from reciprocal measurements in the farfield by multiplication of g^B with $4\pi|\mathbf{x}^B|$ and advancing the time argument by $\frac{|\mathbf{x}^B|}{c}$.

4 Results

Simulated and measured radiation modes as described above have been compared. The configuration is based on a rectangular radiating surface of 60 cm $\times$ 75 cm, consisting of 5 $\times$ 6 elemental radiating surfaces. The simulated radiation mode shapes with the highest efficiencies for frequencies below 450 Hz are shown in Fig. 1. The corresponding measured radiation mode shapes are shown in Fig. 2. It can be seen that there is agreement between the first three shapes. The order of the second shape and third shape is interchanged which is caused by the eigenvalues of these shapes, which are almost equal. Small changes then can lead to a change in the order, which is a relatively harmless phenomenon. The corresponding reductions of the radiated sound power of a vibrating plate can be found in Fig. 3. This result was obtained by using 16 piezoelectric patch actuators and 16 accelerometers. Both the sensors and the actuators were combined in 5 radiation modal sensors/actuators, leading to a reduction of the controller dimensionality. The most important radiation modes for frequencies below 500 Hz were used, taken into consideration the actual excitation of the radiation modes by the structural modes. The controller was based on a 1GHz AMD Athlon processor with RT Linux, using a sampling frequency of 2 kHz. The incident noise used for this experiment was obtained from measurements recorded in-flight in jet aircraft. Since more physical actuators were used than there were independent actuator driving signals, additional constraints were used to determine weighting factors for the actuator array. The design of the array was based on the use of a second set of radiation modes, which were defined in such a way that they were the most efficient radiators at high frequencies while being inefficient radiators at low frequencies. The resulting shapes were used to constrain the output of the actuator array. The results obtained with this method were found to be better than by using constraints on control effort (D.R.Morgan, 1991) or constraints on controller coefficients.

An example with application to active noise barriers for reduction of traffic noise is shown in Fig. 4. Here, the broadband noise produced by 10 independent white noise sources at $z = -2m$ is being reduced at the 2 error microphones in the far field at $z = 30m$. The sampling frequency is 1 kHz. The 15 sensors at $z = -0.5m$ detect the sound radiated from the primary noise sources, which is then used to drive 2 secondary sources at $z = 0.5m$. The sensor signals are processed by radiation modal techniques in order to arrive at a reduction of the controller dimensionality. The radiation modes were obtained from the transfer functions between detection signals and error signals. These transfer functions were obtained by using 20 identification sources at the positions of the primary sources. From the resulting detection signals and error signals the underlying transfer functions were found by causal inversion. The results were obtained with an H_2-optimal multivariable causal prediction technique. For the results of Fig. 4, 2 secondary sources were used. At the error microphones reductions of approximately 12 dB are obtained. However, at other positions increases can be seen. Better results can be obtained if more secondary sources are used, which are constrained by the actuator output at other positions. The result for 2 error sensors, 5 secondary sources and 4 constraint sensors is shown in Fig. 5. Still better results are obtained if more secondary sources and error sensors are used. An example for 8 error

sensors, 8 secondary sources and 4 constraint sensors is given in Fig. 6. The reductions at the error microphones are approximately 18 dB. The order of the latter system is still low because of the use of radiation modal weighting schemes. The techniques can also be applied to asymmetrical configurations. Therefore, the extension to systems in which reductions are to be obtained over larger angular sectors and larger incidence angles is relatively straightforward.

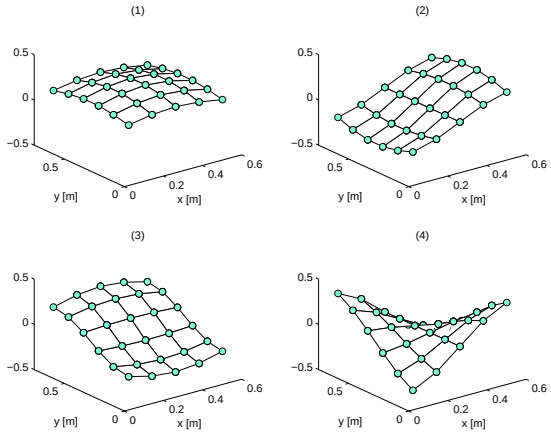

Figure 1: Simulated radiation modes.

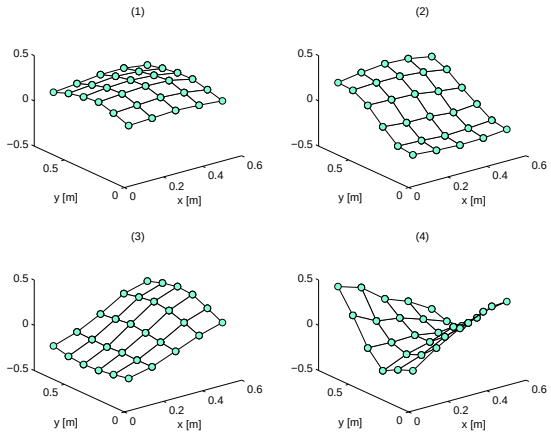

Figure 2: Measured radiation modes.

References

A.D.Pierce (1989). *Acoustics - An introduction to its physical principles and applications*, 2 edn, Acoustical Society of America, Woodbury, New York.

A.P.Berkhoff (2000). Sensor scheme design for active structural acoustic control, *J Acoust Soc Am* **108**: 1037–1045.

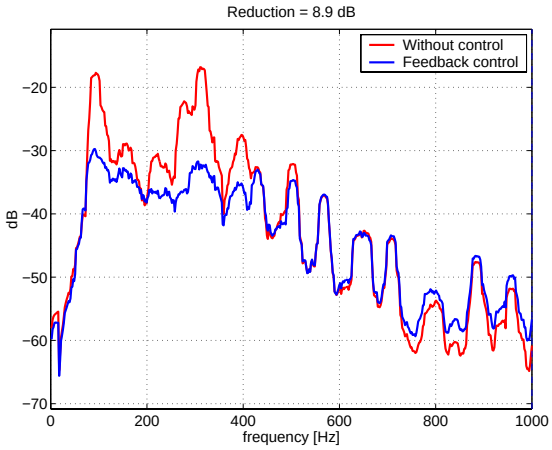

Figure 3: Sound power radiated from an aluminium sandwich panel without control and with control of broadband radiated noise using structural actuators and structural sensors leading to a reduction of 8.9 dB (constant weighting).

A.P.Berkhoff (2002). Broadband radiation modes: estimation and active control, *J Acoust Soc Am*.

A.P.Berkhoff, E.Sarajlic, B.S.Cazzolato and C.H.Hansen (2001). Inverse and reciprocity methods for experimental determination of radiation modes, *in* K.M.Li (ed.), *Proc. ICSV8*, Institute of Acoustics and Vibration.

C.R.Fuller, S.J.Elliott and P.A.Nelson (1996). *Active control of vibration*, Academic Press, London.

D.R.Morgan (1991). An adaptive modal-based active control system, *J Acoust Soc Am* **89**: 248–256.

E.J.J.Doppenberg, A.P.Berkhoff and M.v.Overbeek (2001). Smart materials and active noise and vibration control in vehicles, *in* G.L.Gissinger (ed.), *Proc. IFAC Advances in automotive control*, pp. 205–213.

G.H.Koopmann and J.B.Fahnline (1997). *Designing for quiet structures: a sound power minimization approach*, Academic Press, San Diego.

G.P.Gibbs, R.L.Clark, D.E.Cox and J.S.Vipperman (2000). Radiation modal expansion: Application to active structural acoustic control, *J Acoust Soc Am* **107**: 332–339.

G.V.Borgiotti (1990). The power radiated by a vibrating body in an acoustic fluid and its determination from boundary measurements, *J Acoust Soc Am* **88**: 1884–1893.

M.D.Verweij (1995). Modeling space-time domain acoustic wave fields in media with attenuation: The symbolic manipulation approach, *J Acoust Soc Am* **97**: 831–843.

P.v.Overschee and B.D.Moor (1996). *Subspace identification for linear systems*, Kluwer Academic Publishers, Boston.

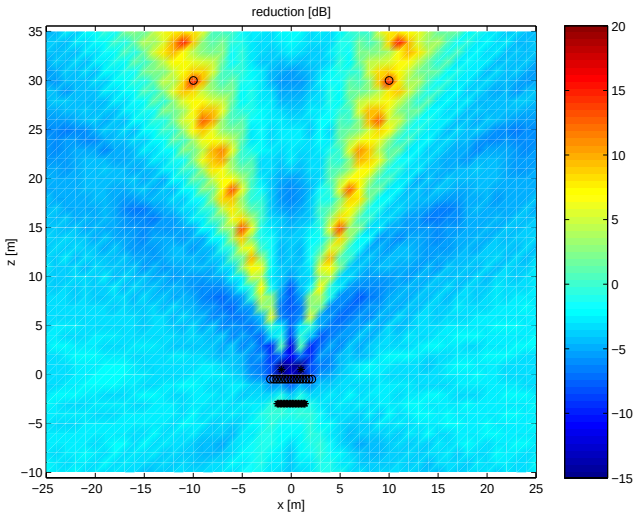

Figure 4: Active noise barrier using 2 error sensors (indicated by 'o' at $z = 30m$), 2 secondary sources (indicated by '*' at $z = 0.5m$). Ten broadband primary noise sources are used (indicated by '*' at $z = -3m$)) and 15 detection sensors (indicated by 'o' at $z = -0.5m$).

S.J.Elliott and M.E.Johnson (1993). Radiation modes and the active control of sound power, *J Acoust Soc Am* **94**: 2194–2204.

W.T.Baumann, W.R.Saunders and H.H.Robertshaw (1991). Active suppression of acoustic radiation from impulsively excited structures, *J Acoust Soc Am* **90**: 3202–3208.

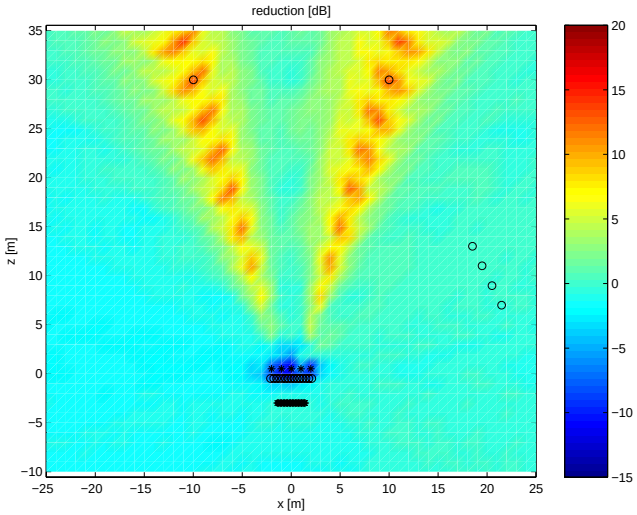

Figure 5: As Fig. 4, using 5 secondary sources (indicated by '*' at $z = 0.5m$) with constraints on 4 microphones (indicated by 'o' at $19m \leq x \leq 21m$) .

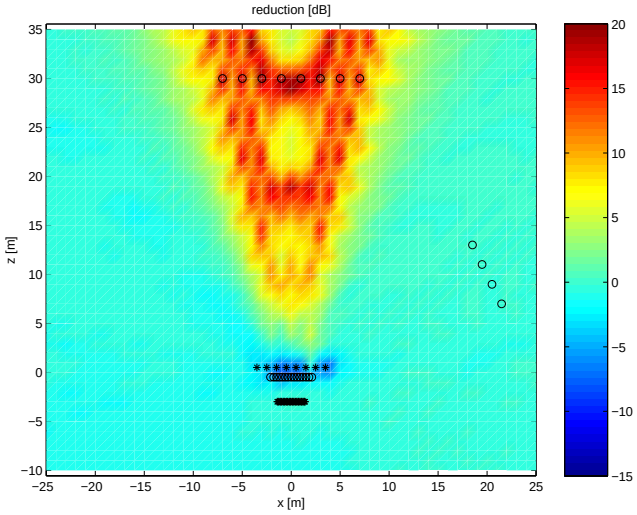

Figure 6: As Fig. 4, using 8 error sensors (indicated by 'o' at $z = 30m$), 8 secondary sources (indicated by '*' at $z = 2m$) and 4 constraint sensors (indicated by 'o' at $19m \leq x \leq 21m$).